buildings

MDPI

Article

A Theoretical Prediction for Shear Capacity of Cellular Solid Shear Walls

Alireza Ghayour Najafabadi [1,2], Parham Memarzadeh [1,*], Tadeh Zirakian [3] and Habib Ghasemi Jouneghani [4]

[1] Department of Civil Engineering, Najafabad Branch, Islamic Azad University, Najafabad 85141-43131, Iran; ghayour.alireza@gmail.com
[2] Department of Civil Engineering, Faculty of Engineering, University of Porto, 4200-465 Porto, Portugal
[3] Department of Civil Engineering and Construction Management, California State University, Northridge, CA 91330, USA; tadeh.zirakian@csun.edu
[4] Department of Civil Engineering, Shahid Rajaee Teacher Training University, Tehran 16788-15811, Iran; ghasemi@sru.ac.ir
* Correspondence: p-memar@iaun.ac.ir

Abstract: Steel plate shear walls (SPSWs) nowadays are accepted as an efficient lateral force-resisting system, especially for high-rise structures, because of their large initial stiffness and high level of energy absorption. There are different types of SPSWs based on their infill plate type. Cellular solid shear walls (CSSWs) are innovative steel shear walls filled with cellular solids. CSSWs can be useful for special architectural designs because of their unique appearance and openings. Whereas many studies have been reported on the SPSWs, there is a shortage of studies about CSSWs. This study presents the results of a detailed, numerical parametric analysis of triangular and quadrilateral CSSWs under monotonic loading in terms of their shear capacity, initial stiffness, and ductility, and also compares them with SPSWs. The investigated parameters are the size of cells, the cellular solid depth, and the cell wall thickness. The study results indicate that at the same capacity, the quadrilateral cellular solids are far lighter than triangular ones, making the quadrilateral CSSWs more suitable for use. In addition, the findings reveal that the performance of CSSWs is good enough to be used as a lateral force-resisting system in buildings. Finally, a practical procedure for the strength capacity of CSSWs based on the theoretical strip model is proposed.

Keywords: theoretical analysis; cellular solid shear wall; parametric study; shear strength prediction

Academic Editor: Grzegorz Ludwik Golewski

Received: 3 December 2024
Revised: 25 December 2024
Accepted: 27 December 2024
Published: 31 December 2024

Citation: Ghayour Najafabadi, A.; Memarzadeh, P.; Zirakian, T.; Ghasemi Jouneghani, H. A Theoretical Prediction for Shear Capacity of Cellular Solid Shear Walls. *Buildings* **2025**, *15*, 106. https://doi.org/10.3390/buildings15010106

1. Introduction

Steel plate shear walls (SPSWs) are a common and efficient lateral force-resisting system that can be used as a single element or with a combination of moment-resisting frames. Such walls can be used in tall buildings considering their initial stiffness, strength, and ductility, as well as their relatively low cost and time of construction [1–8]. Many studies have been conducted in order to evaluate the strength, buckling behavior, and stiffness of SPSW systems and to develop theoretical models [5,9–16].

Numerous studies have investigated various innovative forms of SPSWs aiming to enhance their structural performance. For example, corrugated SPSWs have garnered attention as a novel lateral load-resisting system, as explored in references [17–22]. Corrugated plates present a range of benefits compared to flat plates, such as better energy dissipation capacity, increased ductility, enhanced out-of-plane stiffness, and bolstered buckling stability. Tong et al. proposed a novel composite wall system, the multi-celled corrugated-plate

concrete-filled steel tubular wall, comprising alternating corrugated cells and interval flat plates [23]. The lateral resistance behavior of grid-reinforced steel corrugated shear walls, designed for shear walls with large width-to-height ratios, was also investigated by Dou et al. [24].

Typically, in SPSWs, stiffeners are used around openings in order to limit the shear buckling and preserve the shear capacity of the infill plate [25,26]. However, stiffener fabrication and in situ installation are costly; in addition, inspections are needed to preserve functionality during the wall's lifetime [8]. An architectural alternative to the perforated infill plate of SPSWs is a cellular solid. Cellular solids offer distinct advantages, including the ability to allow natural daylight to pass through, numerous small openings, as well as the efficient installation of various utilities and facilities on a significant scale. Moreover, they can be exposed in the façade of a building or inside the building given their esthetic value.

Recently, the interaction between structure and architecture has led to the introduction of innovative seismic-resistant structural systems that not only create proper stiffness and ductility in structures and prevent inappropriate failure mechanisms, but also provide sufficient space for openings by being installed in the buildinf's facade. For example, in previous years, for the first time in the world, elliptic-braced resisting frames (ELBRFs) were introduced by Ghasemi et al. [27,28], and their seismic behavior was evaluated. This system has appropriate stiffness and high ductility, with an increased response modification factor. Moreover, its energy dissipation is high. In this bracing system, the bracing element is not direct, so the geometric shape of the curved bracing can help to quickly change the internal force of the bracing from compression to tension and vice versa at the moment of lateral load direction change. This makes the curved bracing element act as a ductile fuse and increases the structural system's ductility.

The shape of existing cellular solids in practice is in the form of a honeycomb with prismatic cells or polyhedrons, which are useful in making lightweight structures like sandwich panels or absorbing energy components. The idea of using cellular solids in engineering came from natural materials like wood, cork, bone, and so on [29]. Actually, there are some important mechanical advantages in cellular solid structures that can be useful in tall structures, like high strength/weight ratios and good energy-absorbing capacity [30]. The physical properties of these materials depend on the cell's relative density, topology, and material properties. Triangular and quadrilateral cellular solids are stiffer and more resistant, but absorb less energy than other common cellular solids, such as honeycombs [31]. Such materials are commonly used in industry to improve vehicles' crashworthiness [32].

While cellular solids nowadays are widely used in different fields of engineering, their use as a structural component in civil engineering research is very limited. A cellular solid shear wall (CSSW) is an innovative kind of steel shear wall whose infill plate is replaced by a cellular solid. It is expected that CSSWs are like perforated steel plate shear walls when the size of the perforation is minimized and the number of perforations is maximized [33,34]. The present study has been developed to bridge the gap of knowledge regarding the elastic and inelastic behavior of CSSWs and the effect of cell geometry on their structural behavior. The first objective of this study is to survey the possibility of using CSSWs instead of SPSWs as a lateral force-resisting system. In this order, an extensive analysis of CSSWs with different shapes and sizes of cells, depth of the cellular solid, as well as the orientation and thickness of cell walls is conducted, and the results are compared with those of the SPSW.

Another objective is to develop a theoretical formulation for the ultimate shear strength of CSSWs based on the well-known strip model [35]. In addition, the effect of the geometry

of cells on ultimate shear strength, initial stiffness, ductility, and the weight of 58 CSSW numerical models is discussed.

After this brief introduction, the paper is organized as follows: Section 2 presents the numerical model and its validation. Section 4 shows the parametric analysis results and discussion. An analytical method for calculating the ultimate shear capacity of CSSWs is presented in Section 4. Finally, some conclusive remarks are drawn in Section 5.

2. Numerical Model

Different CSSWs and an SPSW are numerically modeled by the finite element method (FEM) in Abaqus software 6.14-4. To validate the model, the result of the FEM analysis is compared with the experimental test result of the work of Emami et al. [36]. Their test specimen is a single-bay steel shear wall constructed on a 1/2 scale (Figure 1). Table 1 depicts the geometric characteristics of the SPSW specimen. The mechanical properties of the steel used in the beam, column, web plate, stiffeners, and cellular solid are defined in Table 2. The Poisson's ratio and unit weight of steel are, respectively, 0.3 and 7850 kg/m^3.

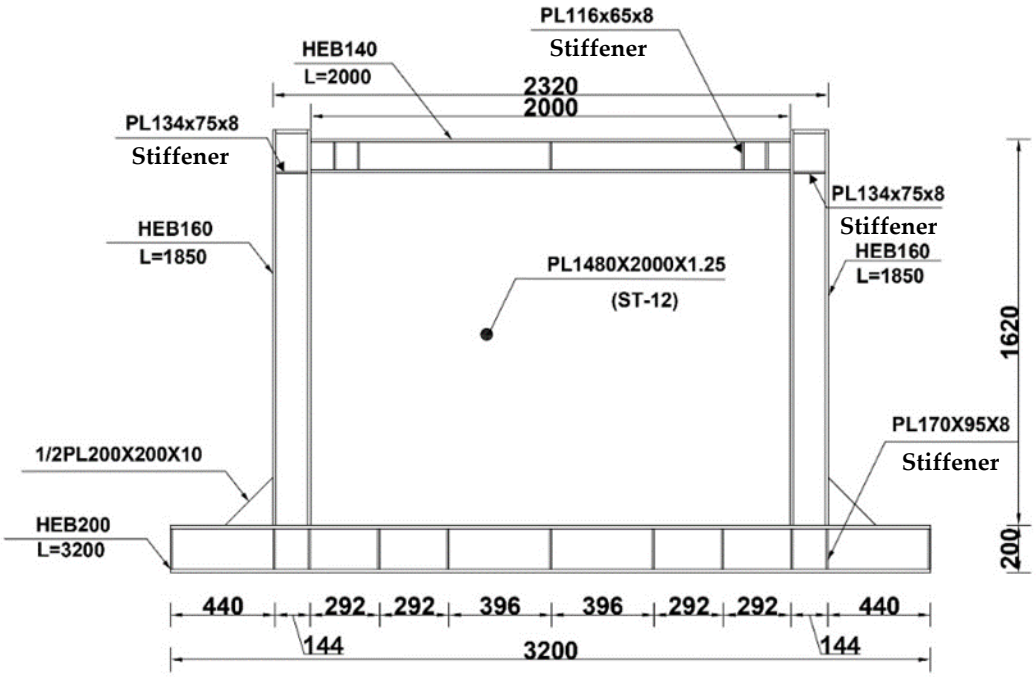

Figure 1. CSPSW test specimen [36].

Table 1. Geometric characteristics of SPSW specimen.

Top Beam	Bottom Beam	Column	Infill Plate Thickness	L/t	h_s/t
HE-B140	HE-B200	HE-B160	1.25	1600	1200

Table 2. Mechanical properties.

Type	Young's Modulus, E (GPa)	Yield Stress, f_y (MPa)	Ultimate Stress, f_u (MPa)	f_y/f_u	Percent Elongation (%)
Infill Web Plate Stiffeners Cellular Solid	210	207	290	0.71	41
Column	210	300	443	0.67	33
Beam	210	288	456	0.63	37

All parts are modeled in a three-dimensional space. The beam and columns are modeled by linear unreduced three-dimensional hexagonal elements (C3D8), and all of the

plates (including the stiffeners, simple infill plate of SPSW, and cellular solids) are modeled by 4-noded reduced integration quadrilateral shell elements (S4R). During the numerical modeling phase, sensitivity analyses indicated that a mesh size ranging from 1 to 5 cm, depending on the cell dimensions, provided suitable convergence in the responses. Therefore, a mesh size of 1 × 1 cm was adopted for the current analysis. This study considers the non-linear geometrical effects of large deformations to achieve higher-accuracy results and reliable analysis. Furthermore, the non-linear stress–strain curve, as shown in Table 3, is employed to model the material behavior accurately, enhancing the realism of the results.

Table 3. Comparison between numerical and theoretical ultimate shear capacities.

Triangular and Quadrilateral Models	Numerical Capacity (kN)	Theoretical Capacity (kN)				Difference for Quadrilateral Models (%)
		V_F	V_t	V_c	V	
T- and Q-45-6.25-10-1.25	1029 and 1026	189	549	283	1021	−0.49
T- and Q-45-8.30-10-1.25	760 and 755	189	427	134	750	−0.53
T- and Q-45-10.0-10-1.25	668 and 661	189	366	79	634	−4.1
T- and Q-45-12.5-10-1.25	573 and 563	189	292	41	522	−7.8
T- and Q-45-16.7-10-1.25	481 and 472	189	220	17	426	−9.7
T- and Q-45-25.0-10-1.25	402 and 396	189	147	4	340	−15.0
T- and Q-45-50.0-10-1.25	317 and 316	189	72	2	263	−17.6
T- and Q-45-12.5-05-1.25	402 and 400	189	146	20	355	−10.8
T- and Q-45-12.5-07-1.25	473 and 465	189	204	29	422	−9.2
T- and Q-45-12.5-10-1.25	573 and 563	189	292	41	522	−7.6
T- and Q-45-12.5-12-1.25	623 and 619	189	350	49	588	−4.9
T- and Q-45-12.5-14-1.25	668 and 662	189	408	58	655	−0.8
T- and Q-45-12.5-10-0.7	430 and 416	189	163	8	360	−14.5
T- and Q-45-12.5-10-1.0	515 and 494	189	233	21	443	−11.2
T- and Q-45-12.5-10-1.25	573 and 563	189	292	41	522	−7.6
T- and Q-45-12.5-10-1.5	629 and 625	189	350	71	610	−2.4
T- and Q-45-12.5-10-2.0	830 and 826	189	466	167	822	−0.5
T- and Q-37-8.30-10-1.25	881 and 860	189	476	191	856	−0.5
T- and Q-37-12.5-10-1.25	631 and 616	189	312	55	556	−9.7
T- and Q-37-16.7-10-1.25	523 and 508	189	228	22	439	−13.6
T- and Q-37-20.0-10-1.25	483 and 467	189	186.9	13	389	−16.7
T- and Q-37-40.0-10-1.25	363 and 330	189	83	1.4	273	−17.3
T- and Q-37-66.7-10-1.25	321 and 301	189	41	0.7	231	−23.3
T- and Q-37-12.5-05-1.25	439 and 410	189	155	28	372	−9.3
T- and Q-37-12.5-07-1.25	509 and 464	189	218	39	446	−3.9
T- and Q-37-12.5-10-1.25	631 and 616	189	312	55	556	−9.7
T- and Q-37-12.5-12-1.25	673 and 640	189	374	66	629	−1.7
T- and Q-37-12.5-14-1.25	720 and 707	189	436	77	702	−0.7
T- and Q-37-12.5-10-0.7	440 and 402	189	174	10	373	−7.2
T- and Q-37-12.5-10-1.0	525 and 490	189	249	28	466	−4.9
T- and Q-37-12.5-10-1.25	631 and 616	189	312	55	556	−9.7
T- and Q-37-12.5-10-1.5	699 and 671	189	374	96	659	−1.8
T- and Q-37-12.5-10-2.0	921 and 918	189	498	224	911	−0.8

The displacement-controlled shear load is monotonically implemented on one side of the top beam following the allowable structure drift (2.5%) [37]. The loading region is considered rigid. This study ignores the effects of gravity loads. All connections between beams, columns, and plates are of the tie connection type. The lower side of the lower beam is restricted in all directions.

This study intends to analyze an SPSW sample, and then the infill web plate is replaced by different cellular solids to study the behavioral differences. The result of the experimental work of Emami et al. [36] on a one-story single-bay half-scale SPSW is used to compare

with the FEM numerical result (Figures 2 and 3). This comparison depicts, with about 90% accuracy, the FEM results for the ultimate capacity, which signals a successful validation.

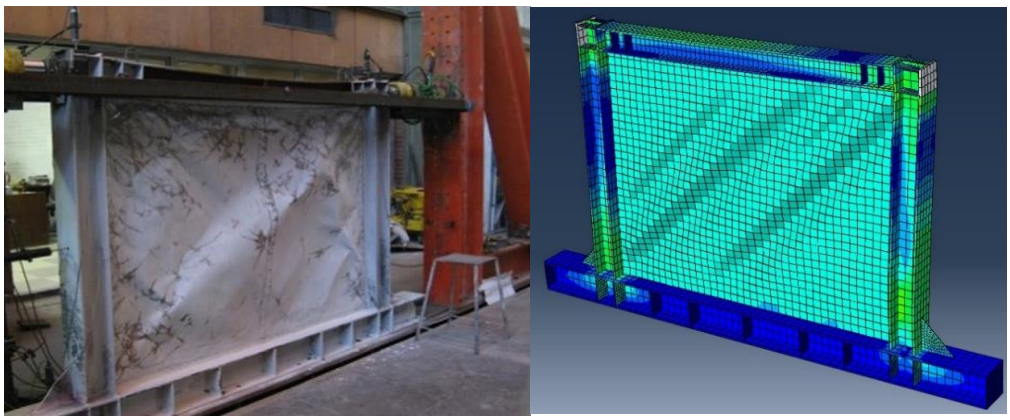

(**a**) (**b**)

Figure 2. Comparison of experimental and numerical deformations of SPSW. (**a**) Experimental specimen [36]. (**b**) FEM model.

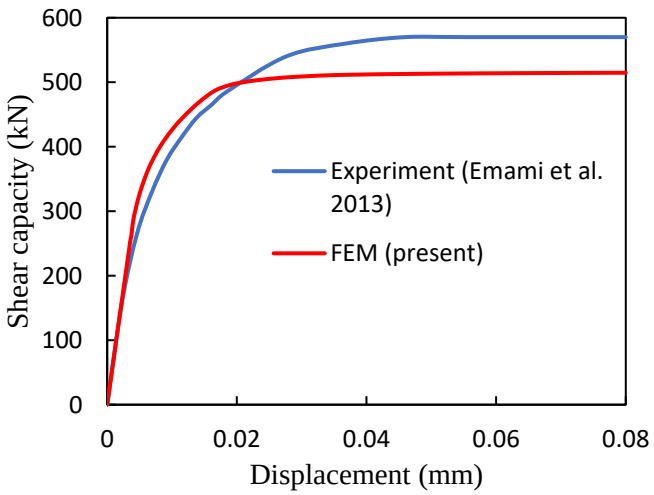

Figure 3. Force–displacement curves of SPSW [36].

The experimental buckled shape present in Figure 2a is very similar to the ones obtained with the model and shown in Figure 2b.

The CSSW models are analyzed under pushover loading up to a 2.5% drift angle at the top of the frame. The effect of different parameters, including the cell size, cellular solid depth, and cell wall thickness, is discussed as follows.

3. Parametric Analysis

In order to perform a parametric study, a total of 58 single-story CSSWs are analyzed. The CSSW models are denoted based on the geometry of the cells (Figure 4) as "*S*-*α*-*l*-*d*-*t*", where *S* specifies the shape of the cells (T for triangular and Q for quadrilateral cells); α is the slope angle of the inclined cell walls, which is 37° and 45° in the present study; *l* is the length of triangular cell base or the horizontal diameter of quadrilateral cells in centimeters; *d* is the depth of cellular solid in centimeters; and *t* is the cell wall thickness in millimeters.

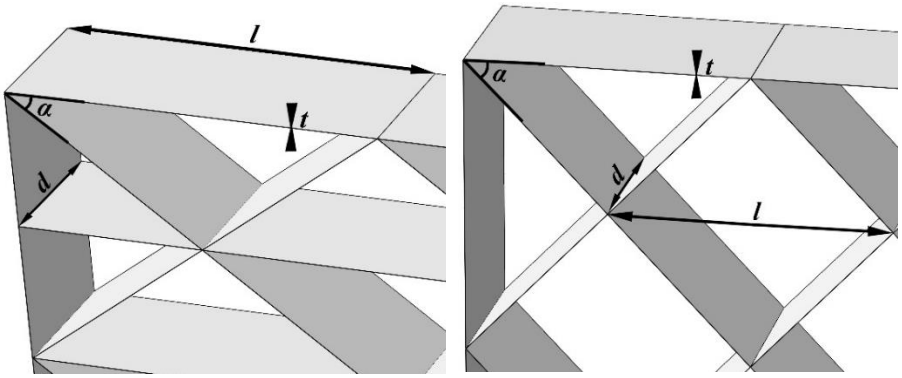

(**a**) (**b**)

Figure 4. Geometry of CSSW models. (**a**) Triangular. (**b**) Quadrilateral.

3.1. Effect of Cell Size

Figure 5 shows the force–drift curves of triangular and quadrilateral CSSWs with different cell sizes for $\alpha = 45°$ and $\alpha = 37°$, respectively.

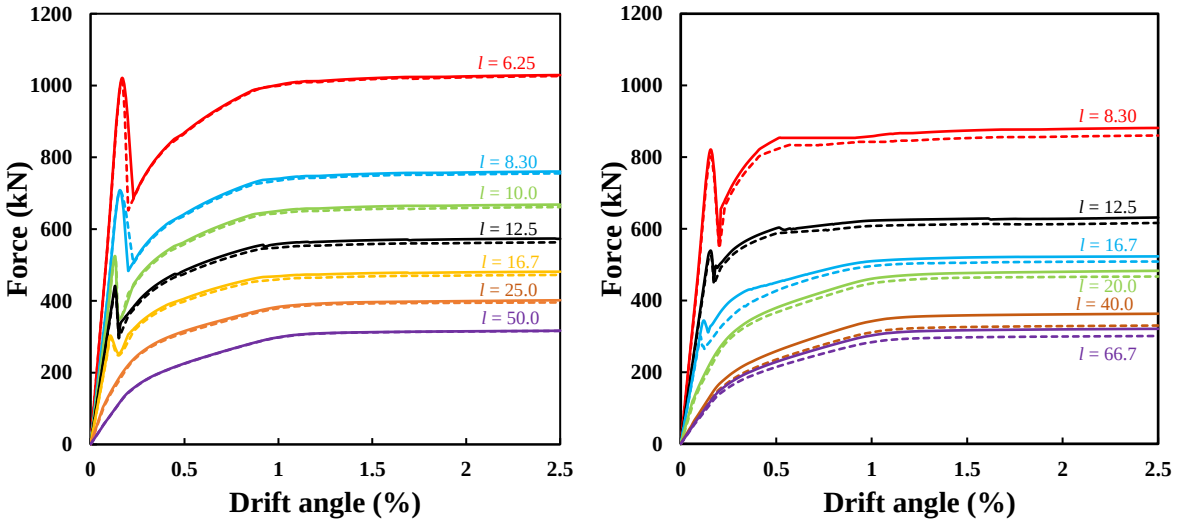

(**a**) (**b**)

Figure 5. Force–drift curves of T- and Q-*α*-*l* (variable)-10-1.25 for (**a**) $\alpha = 45°$ and (**b**) $\alpha = 37°$ (line: triangular; dash: quadrilateral).

As can be seen in Figure 5, some of the force–drift curves experience a huge drop. The reason for this drop is buckling in the compressive cell walls. With the start of lateral loading, the force and displacement increase linearly up to the occurrence of the first buckling in compressive members; then, the drop occurs. The buckling extends over other compressive members until the participation of the compressive members in bearing the shear load is lost, and the tensile members bear almost the whole shear load. This point is the end of the drop, followed by an upward trend in the force–drift angle curve. For instance, von Mises stresses coupled with rotational displacement components (UR) of Q-37-16.7-10-1.25 are represented in Figure 6. As shown in Figure 6a, at the start of drop, buckling of cell walls occurs in two areas (surrounded by red circles). During the drop, the rotation angle of buckling in compressive members increases, and some other members buckle as well until the end of the drop (Figure 6b). It is understood from von Mises stress that as buckling starts, the absorption of plastic energy starts as well. As a result, the start of the drop is assumed as the yielding point for the calculation of the ductility in this study.

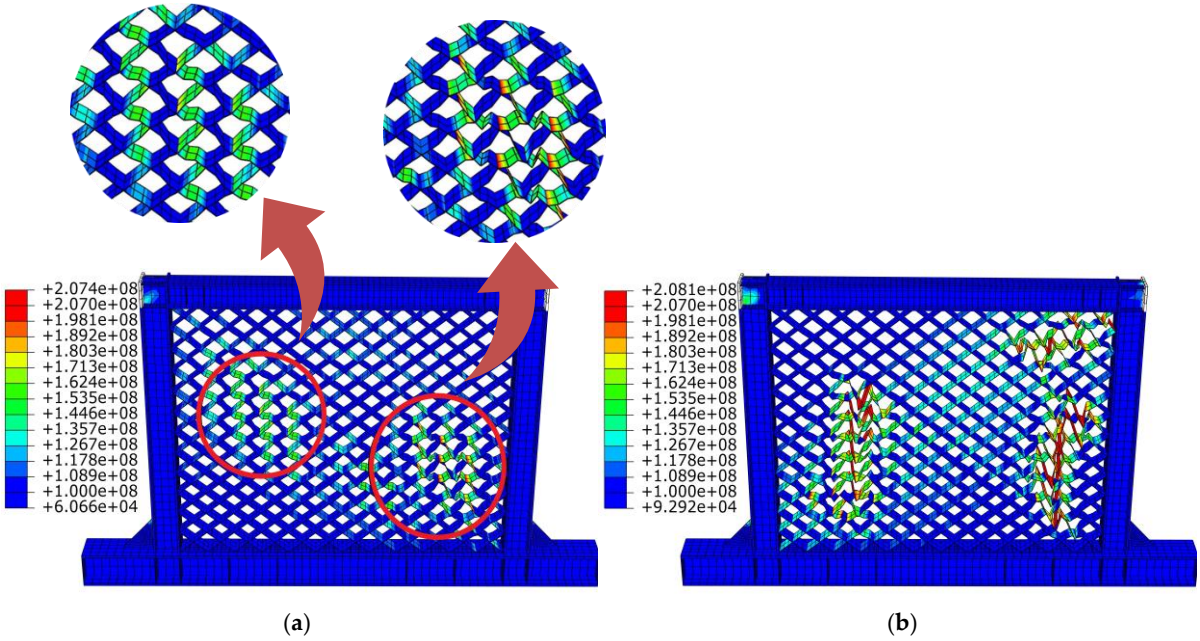

(**a**) (**b**)

Figure 6. Von Mises stress (N/m^2) and rotational displacement components of Q-37-16.7-10-1.25 at (**a**) initiation of drop and (**b**) end of drop.

The size of cells in triangular and quadrilateral cellular solids is, respectively, expressed according to the length of the triangle base and the length of the horizontal diameter of the quadrilateral, denoted by "*l*". Figure 7 presents the effect of cell size on the behavior of CSSWs. According to Figure 7a, the shape of cells (triangular or quadrilateral) has a negligible impact on the ultimate strength of CSSWs. When the cell size increases, the ultimate capacity exponentially decreases, such that, as the cell length (*l*) increases eightfold, the capacity decreases by around 65%. The results for the stiffness are depicted in Figure 7b. As seen, the initial stiffness has a relatively high sensitivity to the cell size, and with the increase in the cell size, it decreases up to 89%.

In this study, ductility is precisely defined as the ratio of the displacement corresponding to the ultimate force to the displacement at yield. According to FEMA P-58-1 guidelines, the ultimate capacity often considered the collapse point, aligns with the excessive lateral displacement point. This critical juncture signifies a state where the structure experiences a near-complete loss of lateral stiffness, potentially leading to the failure of crucial vertical-load-carrying components [38]. To ensure meaningful comparisons among the diverse models examined in this research, a standardized approach to ductility calculation is employed. Here, the yielding point is identified as the termination of the linear segment of the pushover curve, indicating the initiation of plastic deformation. Additionally, the ultimate point is pinpointed as the moment when the tangent of the curve becomes horizontal, signifying zero lateral stiffness. This meticulous methodology guarantees precise evaluation and the comparison of ductility across the various structural models investigated in this study. The variation in ductility with cell size is illustrated in Figure 7c. By a rough estimation, it can be said that with a change in the cell size in the range studied here, the ductility of CSSWs changes almost between 3.3 and 8.4. The T- and Q-45-25-10-1.25, as well as the T- and Q-37-16.7-10-1.25 exhibit the highest ductility in their corresponding category.

The capacity-to-weight ratio of CSSWs versus the cell size is shown in Figure 7d. It is found that cellular solids with large cell sizes have a higher capacity-to-weight ratio. In addition, quadrilateral specimens have capacity-to-weight ratios that are 18 to 79% higher than triangular specimens. As a result, the use of quadrilateral CSSWs can be justifiable in terms of the amount of steel consumed.

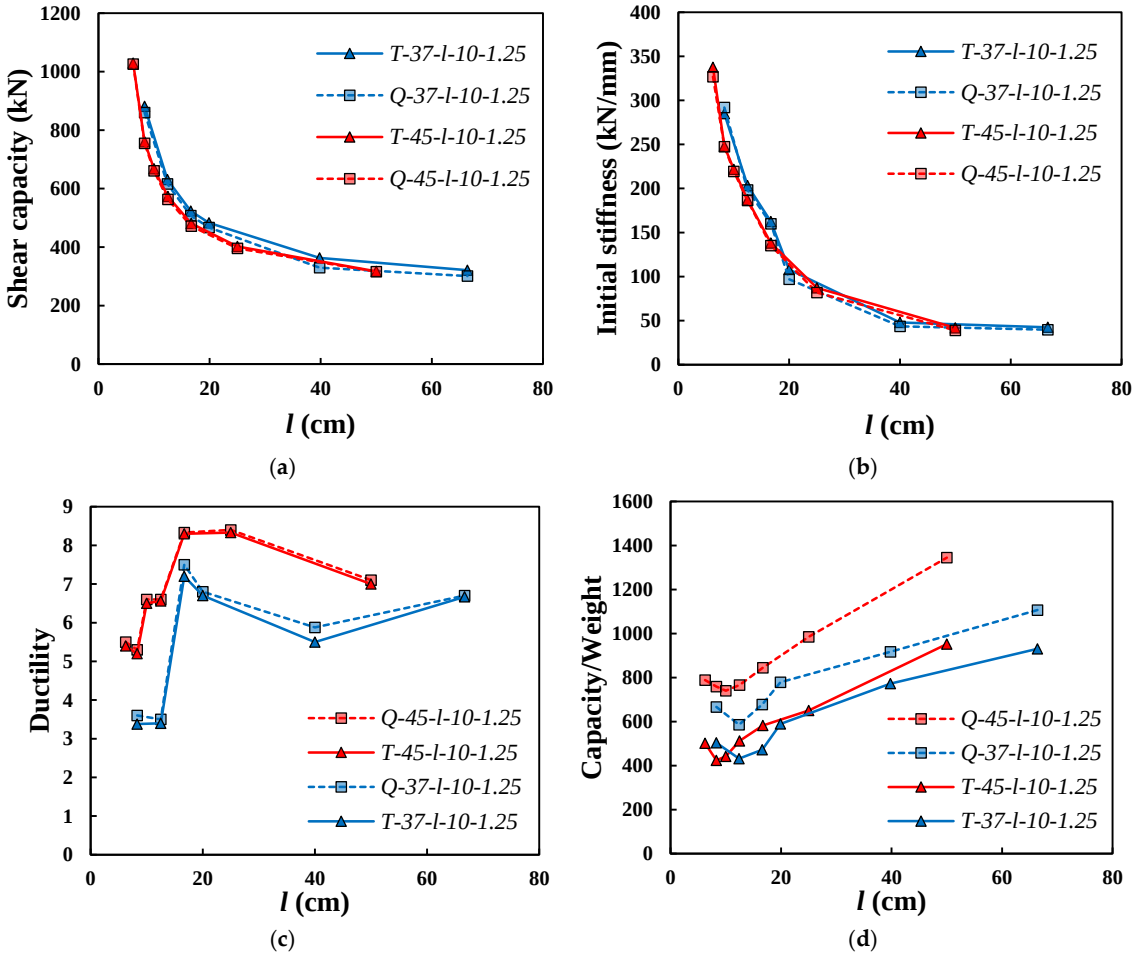

Figure 7. Comparison between T- and Q-45-*l* (variable)-10-1.25 CSSWs for (**a**) shear capacity, (**b**) initial stiffness, (**c**) ductility, and (**d**) C/W (Capacity/Weight).

3.2. Effect of Cellular Solid Depth

Figure 8 illustrates the force–displacement curves of triangular and quadrilateral CSSWs with different cellular solid depths for $\alpha = 45°$ and $\alpha = 37°$, respectively. As expected, an increase in the element depth produces an increase in the strength of the structure.

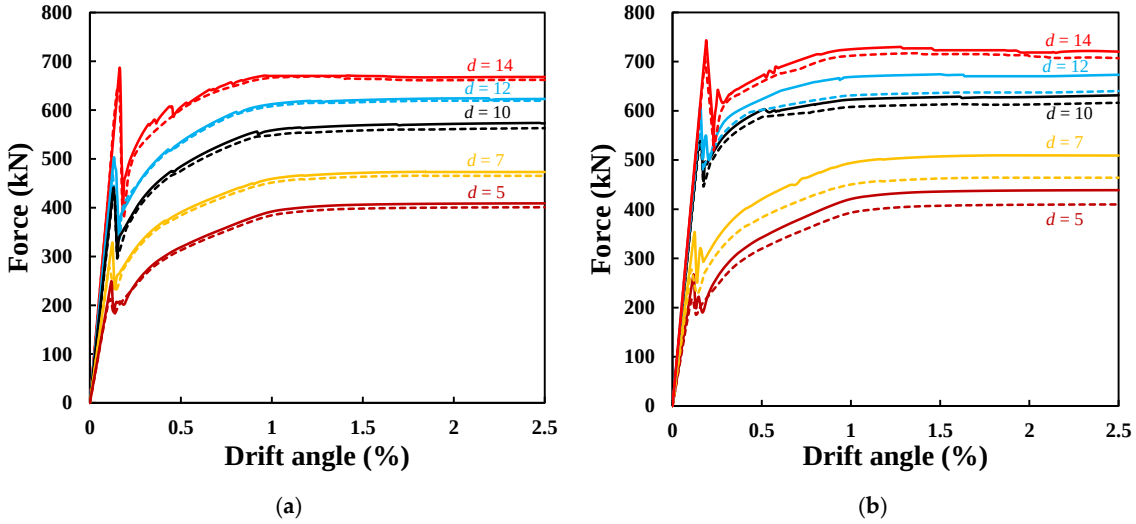

Figure 8. Force–drift angle curves of T- and Q-*α*-12.5-*d* (variable)-1.25 for (**a**) $\alpha = 45°$ and (**b**) $\alpha = 37°$ (line: triangular; dash: quadrilateral).

Figure 9 demonstrates the comparison of CSSW behavior with different cellular solid depths. For this purpose, cellular solids with depths of 5, 7, 10, 12, and 14 cm are studied. As expected, increasing the cellular solid depth somewhat linearly leads to an increase in the ultimate shear capacity of CSSWs, such that by increasing the cellular solid depth about three times, the capacity increases by 1.75 times. However, there is not much difference between the shear capacities of triangular and quadrilateral CSSWs (Figure 9a).

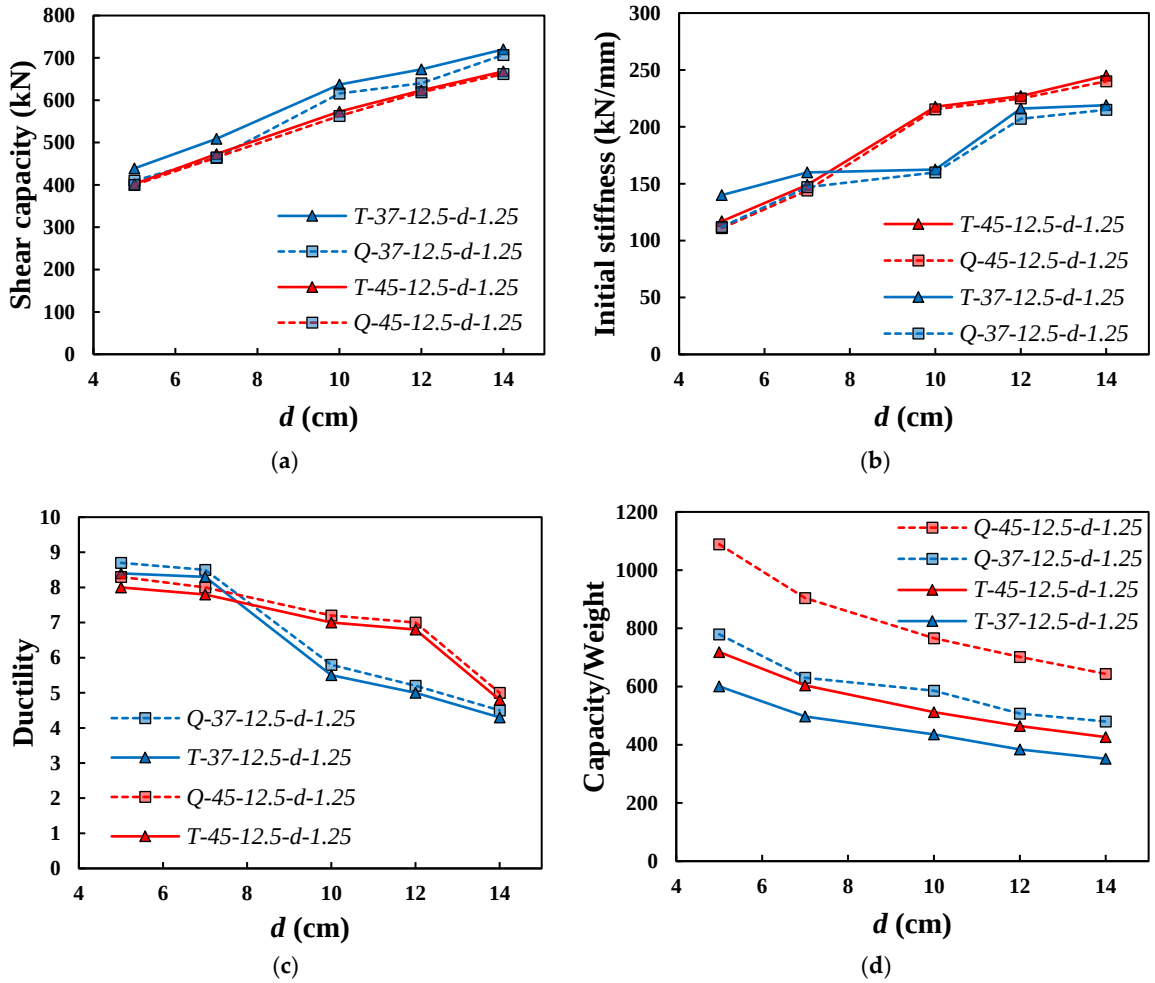

Figure 9. Comparison between T- and Q-45-12.5-*d* (variable)-1.25 CSSWs for (**a**) shear capacity, (**b**) initial stiffness, (**c**) ductility, and (**d**) C/W.

According to Figure 9b, an increase in the cellular solid depth leads to a dramatic rise in the initial stiffness of the CSSW. It is essential to mention that the initial stiffness of triangular cellular solids could be 5 to 35 percent higher than that of quadrilateral cellular solids. The increase in the depth of the cellular solid decreases the ductility. In addition, overall, quadrilateral models have better ductility compared to triangular ones (Figure 9c).

Moreover, the rise in depth linearly decreases the C/W ratio of the cellular solids. However, as expected, regarding this parameter, the performance of quadrilateral CSSWs is more satisfying (Figure 9d). Apart from that, if the cellular solid depth is 5 cm or less, then the whole cellular solid goes through the out-of-plane buckling, while in thicker cellular solids, only the wall of cells experiences the buckling (Figure 10).

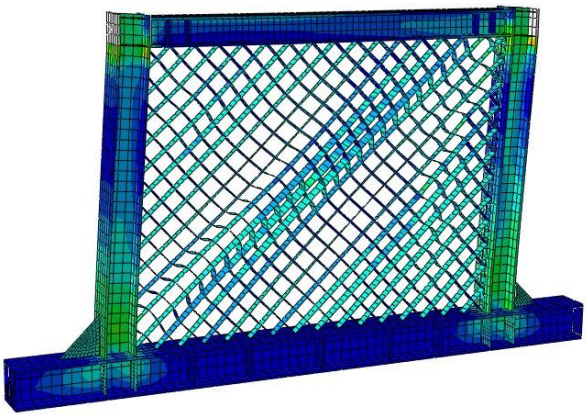

Figure 10. Out-of-plane buckling of Q-45-12.5-5-1.25.

3.3. Effect of Cell Wall Thickness

Figure 11 illustrates the behavior of CSSWs with different cell wall thicknesses. For this purpose, cellular solids with wall thicknesses of 0.7, 1.0, 1.25, 1.5, and 2.0 mm have been compared. In Figure 12, it is evident that an increase in thickness negatively affects the ductility of a shear wall. However, this rise significantly enhances both the ultimate strength and initial stiffness. Additionally, the C/W ratio of the CSSWs exhibits a decreasing trend with the augmentation of cell wall thickness. Similar to other models, it is observed that the C/W ratio of triangular models is notably lower than that of quadrilateral ones. This difference is attributed to the presence of horizontal cell walls.

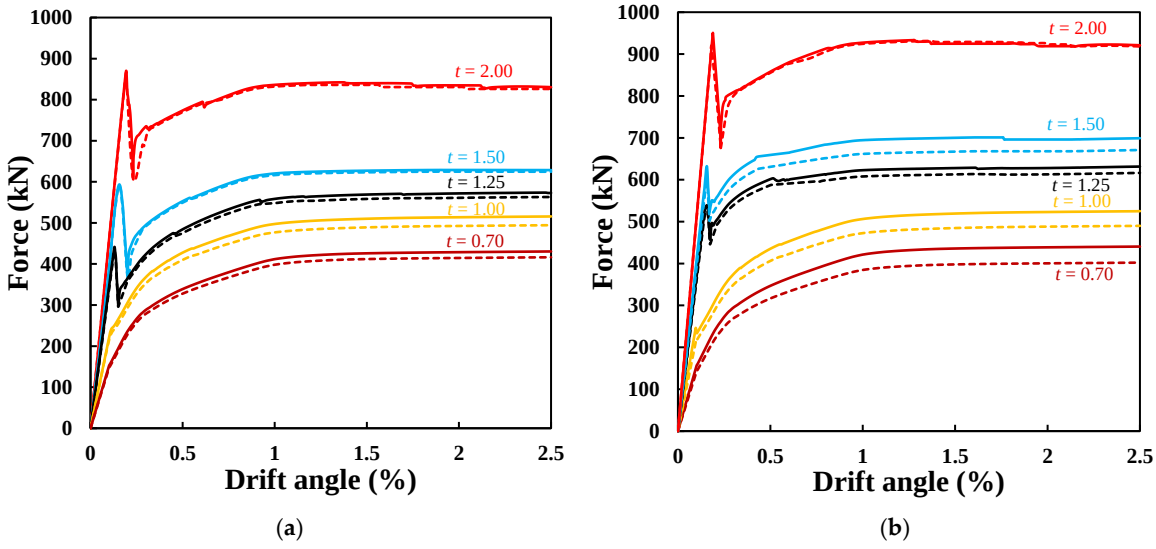

Figure 11. Force–drift angle curves of T- and Q-α-12.5-10- t (variable) for (**a**) $\alpha = 45°$ and (**b**) $\alpha = 37°$ (line: triangular; dash: quadrilateral).

3.4. Comparison of CSSW and SPSW

A comparison is undertaken between an SPSW and CSSWs that have the closest shear capacity to the SPSW. These CSSWs are T- and Q-37-16.7-10-1.25 as well as T- and Q-45-12.5-10-1.0. By comparing the models, it is found that the CSSWs with relatively the same capacity as the SPSW have higher initial stiffness compared to the SPSW, and as seen in Figure 13, they reach the yielding limit in a lower drift. Regarding the absorption of plastic energy, the considered cellular solids have equal or greater plastic energy compared to the SPSW (Figure 13).

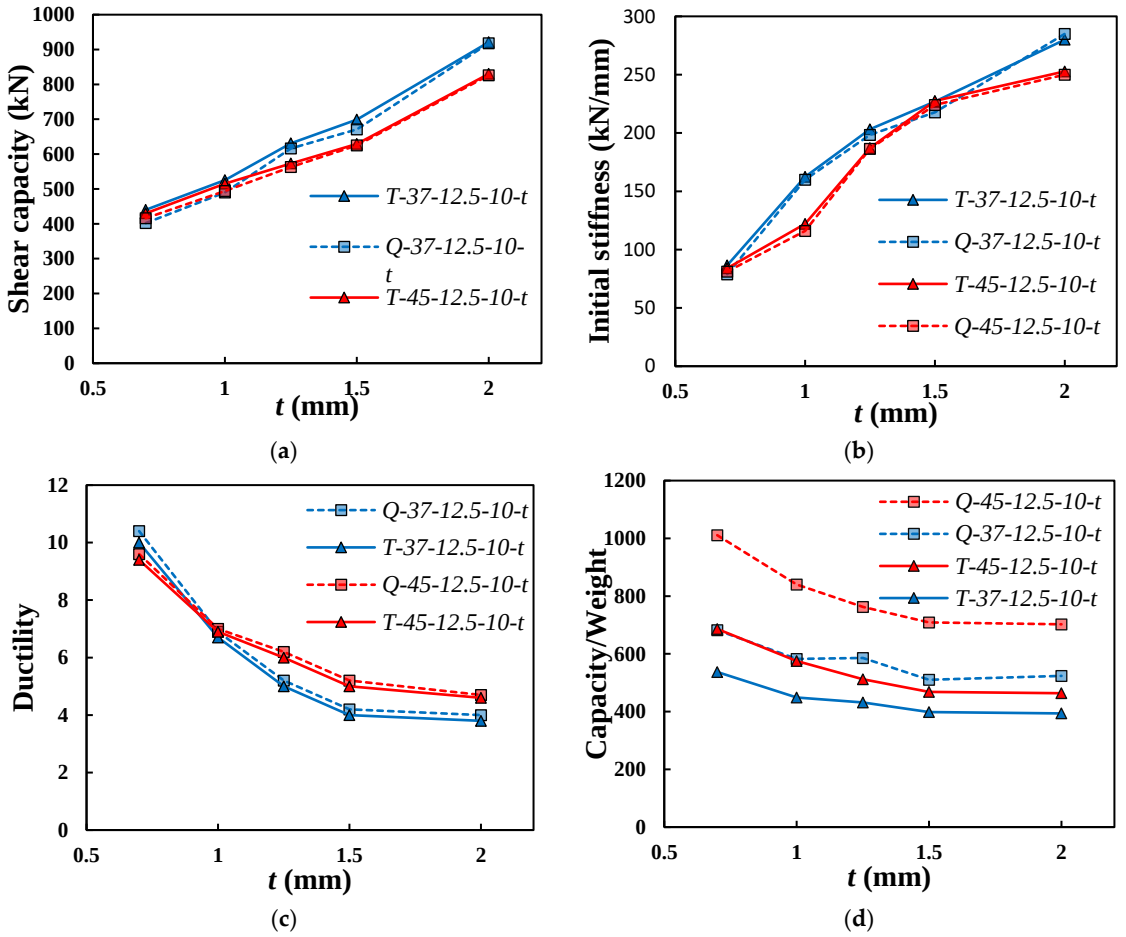

Figure 12. Comparison between T- and Q-45-12.5-10- *t* (variable) CSSWs for (**a**) shear capacity, (**b**) initial stiffness, (**c**) ductility, and (**d**) C/W.

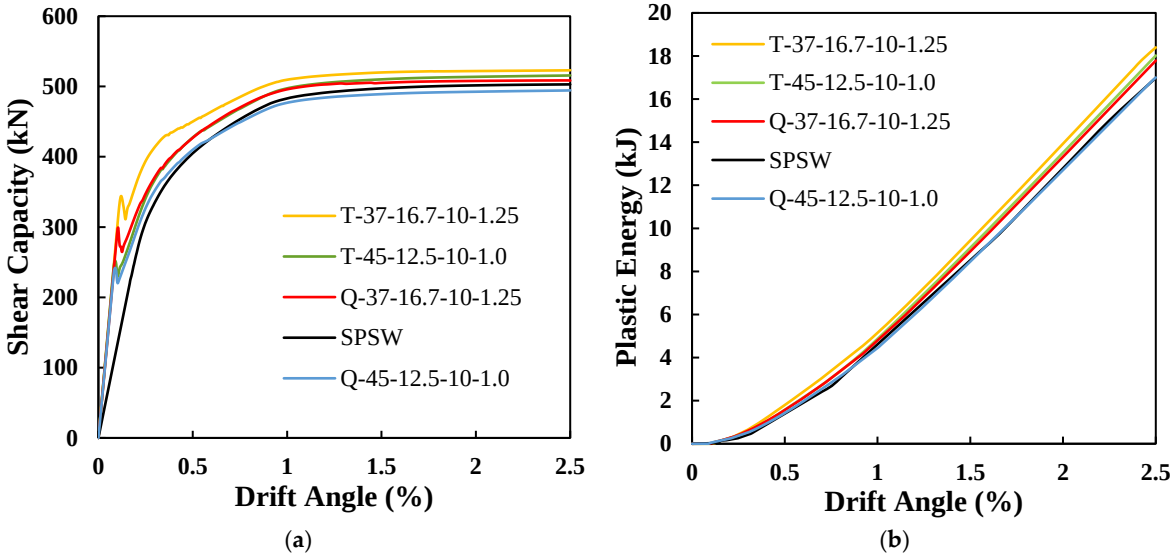

Figure 13. Comparison between (**a**) load–displacement curves and (**b**) plastic energy of four CSSWs and an SPSW.

In SPSWs, the buckling of the infill plate creates a tension field that provides resistance to the shear loads. Unlike SPSWs, the CSSWs are probably less prone to global buckling; but local buckling is very possible in the thin compressive wall of the cells. In this way, a large part of the CSSW shear load is borne by the tensile cell walls. The tension stresses

in the cell walls play the role of the tension field of SPSWs. However, it is possible for CSSWs to postpone the compressive buckling by reducing the slenderness of cell walls, and therefore, compressive and tensile cell walls would have a more or less equal contribution to CSSW shear strength before cell wall buckling.

3.5. Structural Behavior of CSSWs

Observing the plastic strain growth in cellular solids, interesting findings are achieved which are mostly similar in all cellular solids. In the first stage, the force–drift curve is linear. However, it is not linear anymore after the first buckling in the compressive elements. It should be considered that there is probably imperfection in the fabrication of CSSWs which leads to early buckling in compressive elements. After buckling, the tensile elements start yielding by increasing the lateral load. Tensile elements start to yield from the part of the cellular solid where compressive cell walls buckle first. Then, other tensile elements meet yielding stress quickly. Almost all tensile elements finally yield due to the reticular structure of cells while none of the tensile or compressive walls reach the ultimate stress. As an example, the plasticity growth and Von Mises stress of T-37-12.5-10-1.25 and Q-45-12.5-10-1.25 are illustrated in Figures 14–17. Actually, it is understood that the horizontal members in triangular cellular solids (base of triangles) do not have a considerable contribution in bearing the shear loads and do not reach the yielding stress even in the highest amount of drift (Figures 15 and 17). So, there is not much difference between the ultimate strength of triangular and quadrilateral cellular solids but the quadrilateral ones are much lighter in weight.

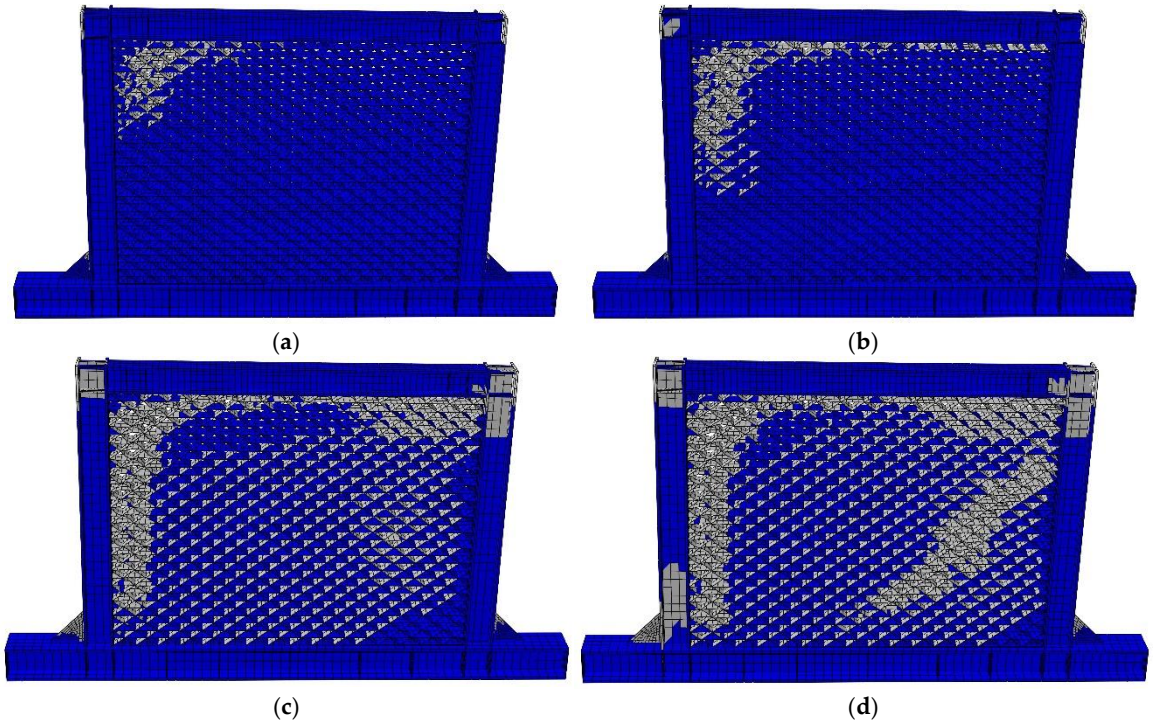

Figure 14. Plasticity growth of T-37-12.5-10-1.25: (**a**) 0.25% drift, (**b**) 0.50% drift, (**c**) 1.25% drift, and (**d**) 2.50% drift.

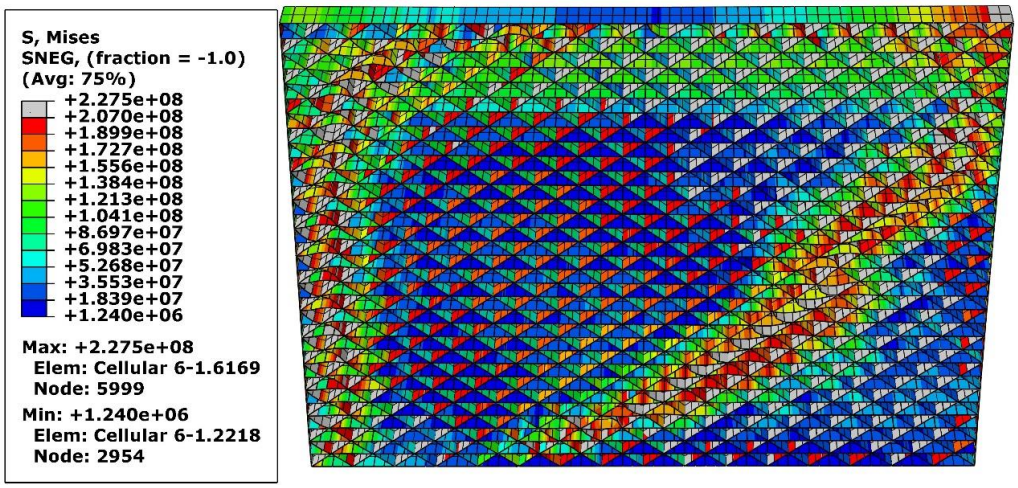

Figure 15. Von Mises stress of T-37-12.5-10-1.25 at 2.5% drift angle.

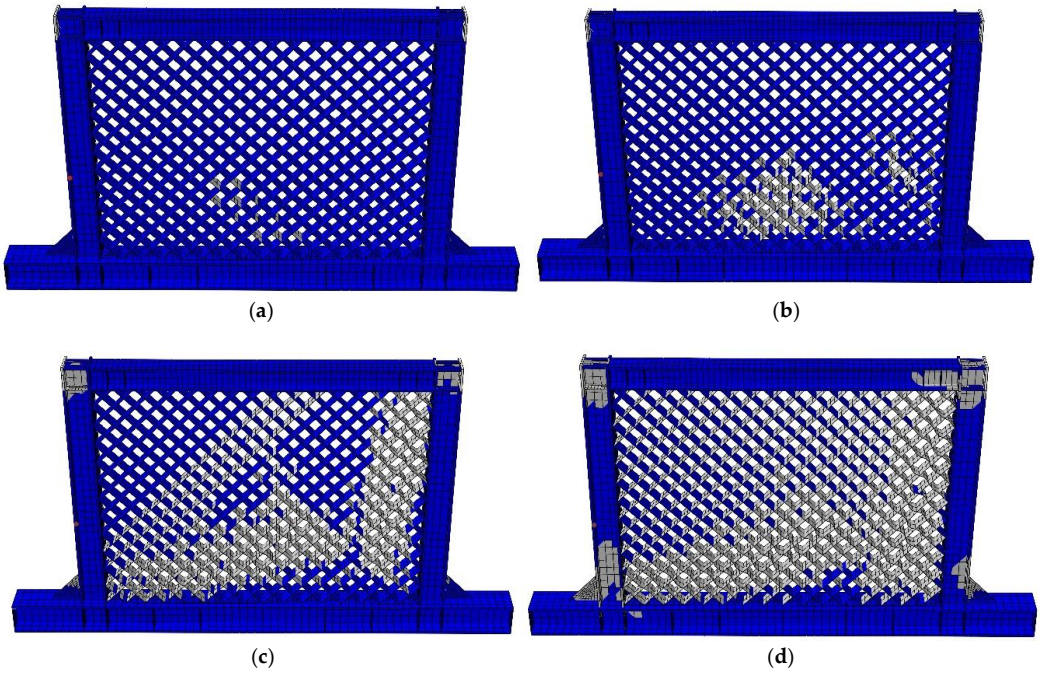

Figure 16. Plasticity growth of Q-45-12.5-10-1.25: (**a**) 0.25% drift, (**b**) 0.50% drift, (**c**) 1.25% drift, and (**d**) 2.50% drift.

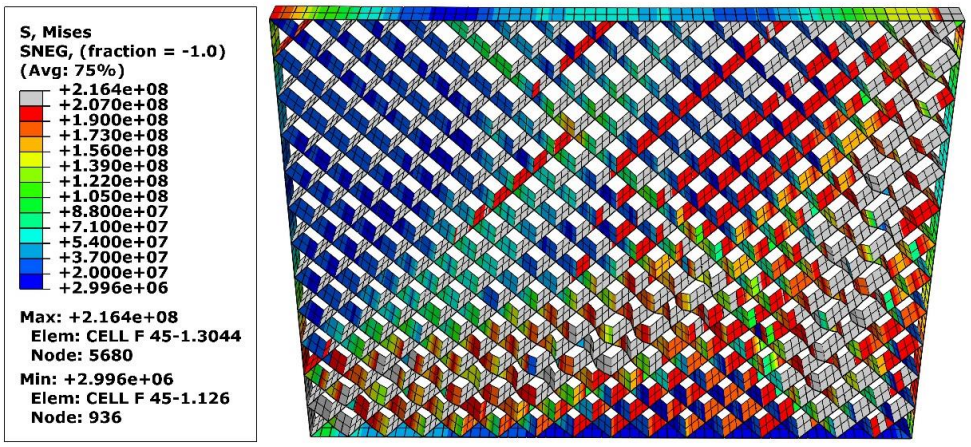

Figure 17. Von Mises stress of Q-45-12.5-10-1.25 at 2.5% drift angle.

4. Analytical Model

In the following section, the theoretical method outlined for determining the ultimate shear capacity of CSSWs incorporates an innovative approach inspired by the widely recognized strip model [35]. This methodology stems from examining the behavior exhibited by cell walls, treated as strips, when subjected to lateral loads. Unlike the conventional approach, our method introduces both tensile and compressive strips. This distinction arises because, when cellular solids experience shear forces, some cell walls face compression, while others undergo tension. It is also crucial to consider buckling in the compressive cell walls during this analysis.

While studying the FEM analysis of triangular cellular solids, it is understood that the horizontal cell walls (the base of triangles) do not have a notable contribution to bearing the shear loads. Thus, the strength of horizontal cell walls can be ignored in calculating the shear capacity of triangular CSSWs in this approach. Herein, the shear capacity of a triangular CSSW is assumed to be equal to its corresponding quadrilateral one. This assumption has conservative results for the shear capacity.

In the present study, the following equation is proposed for calculating the ultimate shear capacity of CSSWs:

$$V = (V_t + V_c) + V_F \tag{1}$$

in which V_t, V_c, and V_F are the shear loads borne by the tensile cell walls, compressive cell walls, and frame, respectively, which will be explained below.

Using the strip model, V_t could be calculated from the following equation:

$$V_t = \sum_{i=1}^{k} \frac{d_i F_t}{h_s} + \sum_{j=1}^{m} F_t sin\alpha + \sum_{i=1}^{n} \frac{d_i F_t}{h_s} \tag{2}$$

According to Figure 18, k, m, and n represent the numbers of tensile strips (tensile cell walls) in zone 1, zone 2, and zone 3 (in this study, $n = k$); F_t is the tensile force of each wall which is assumed to be equal to the plate yield stress times the cross-sectional area of cell walls; d_i in zones 1 and 2 is the distance of each cell wall to the upper left beam-to-column joint; d_i in zone 3 is the distance of each cell wall to the lower right beam-to-column joint; h_s is the height of the infill cellular solid; and α is the positioning angle of oblique cell walls that are 37° or 45° degrees in this study.

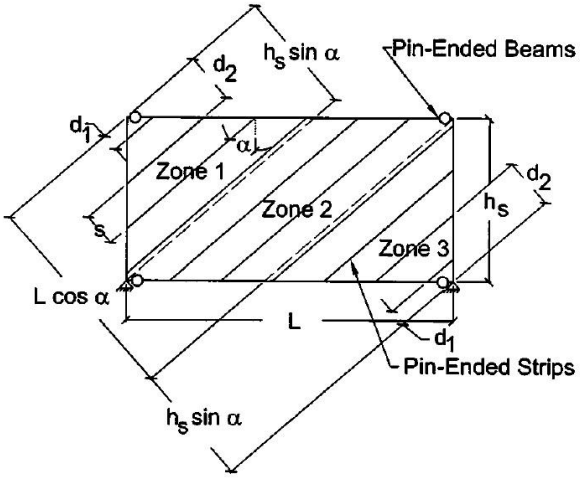

Figure 18. Single-story strip model [35].

V_c can be calculated from the following equation:

$$V_c = \sum_{i=1}^{k} \frac{d_i F_c}{h_s} + \sum_{j=1}^{m} F_c \sin\alpha + \sum_{i=1}^{n} \frac{d_i F_c}{h_s} \tag{3}$$

where k, m, and n represent the numbers of compressive strips (compressive cell walls) in zone 1, zone 2, and zone 3 (Figure 18). F_c is the compressive load of cell walls by considering the buckling effect which is achieved based on the following equation [39]:

$$F_c = F_{cr}\, A_g \tag{4}$$

where A_g is the cross-sectional area of cell walls. F_{cr} represents the critical stress (considering buckling effect) which can be calculated from the following equation:

$$F_{cr} = \begin{cases} \left[0.658^{\frac{F_y}{F_e}}\right] F_y \; if \; \lambda \leq 4.71\sqrt{\frac{E}{F_y}} \\ 0.877\, F_e \; if \; \lambda > 4.71\sqrt{\frac{E}{F_y}} \end{cases} \tag{5}$$

where F_y is the yielding stress and E represents the elastic modulus. λ (slenderness ratio) and F_e (Euler stress) are defined as below:

$$F_e = \frac{\pi^2\, E}{\lambda^2} \tag{6}$$

$$\lambda = \frac{K l_c}{r} \tag{7}$$

where KL_c is the distance between the points of zero moment, or inflection points along the length. The length KL_c is known as the effective length of the compressive members. The dimensionless coefficient K is called the effective length factor. In the present study, in order to capture conservative results, the K factor is assumed to be equal to 1; l_c is the length of cell walls; and r is the radius of gyration.

V_F could be obtained from the following equation [40]:

$$V_F = \frac{4\, M_p}{h_s} \tag{8}$$

in which M_p is the smaller of the beam and column plastic moments.

In Table 3, a comparison between the results of ultimate shear capacity obtained from the numerical analysis and from the proposed theoretical formula is presented. As mentioned before, the shear capacity of triangular cellular solids obtained from the formula is similar to their comparable quadrilateral cellular solids due to the insignificant contribution of horizontal cell walls in load-bearing.

5. Summary and Conclusions

In the current study, the behavior of an SPSW and a number of CSSWs with different geometries of cells has been investigated both numerically and analytically.

Our primary objective was to explore the structural performance of CSSWs as a novel system. The comparison made in Section 3.4 is to illustrate the basic structural differences rather than to assert a comprehensive superiority of CSSWs over SPSWs. Although CSSWs are heavier compared to SPSWs, non-structural considerations, such as aesthetics, light transmission, and the ease of utility installations, represent qualitative advantages that CSSWs have over traditional SPSWs. While these advantages may not lend themselves to direct quantitative comparison, they hold significant relevance in the architectural design of tall buildings. Therefore, they should be carefully weighed alongside structural performance in practical decision-making.

The focus of the paper is on the parametric investigation of CSSWs under monotonic loading to establish a fundamental understanding of the system's performance in terms of shear capacity, stiffness, and ductility, which are critical parameters in the design of lateral

force-resisting systems. This initial phase aimed to explore the influence of geometric parameters on the structural behavior of CSSWs in a controlled manner, providing a basis for more complex studies, such as those involving cyclic loads. The results showed that CSSWs have the potential to be used as a lateral load-resisting system in buildings as their performance is so close to that of SPSWs. For a more comprehensive assessment of the CSSW's performance, especially in seismic applications, cyclic behavior must be analyzed to simulate the load reversal characteristics experienced during an earthquake.

The analytical approach inspired by the strip model was developed to calculate the ultimate shear capacity of each CSSW. The results demonstrated that the shear capacity calculated by the analytical approach is consistently 0.5% to 20% more conservative when compared to the FEM method. The difference between the ultimate shear capacity obtained through the analytical and FEM methods decreases in CSSWs with higher ultimate strength.

The behavior and properties of CSSWs can be modified by changing the geometry of cells. The following observations and conclusions are drawn from the study on the effects of changes in cell geometry on the performance of CSSWs:

- The ultimate shear capacity of triangular CSSWs is close to that of their quadrilateral counterparts, while triangular CSSWs are 30 to 60% heavier. Apart from that, the initial stiffness of triangular CSSWs is considerably higher than that of quadrilateral ones.
- By increasing the depth of cellular solids or cell wall thickness, the ultimate shear strength of CSSWs is increased. Another way of increasing shear capacity is by reducing the size of cells.
- Initial stiffness has a direct relation with the depth of the cellular solid and the thickness of the cell walls. However, it declines with an increase in the size of the cells.
- An interesting point about using CSSWs is that, due to their geometry, almost all cell walls pass yielding stress, while none of them reach ultimate stress.

Author Contributions: Conceptualization, P.M.; Methodology, P.M.; Software, A.G.N.; Validation, A.G.N.; Formal analysis, A.G.N.; Investigation, A.G.N.; Resources, P.M. and T.Z.; Writing—original draft, A.G.N.; Writing—review & editing, P.M., T.Z. and H.G.J.; Supervision, P.M. All authors have read and agreed to the published version of the manuscript.

Funding: This research received no external funding.

Data Availability Statement: Data are contained within the article.

Conflicts of Interest: The authors declare no conflict of interest.

References

1. Mondal, M.A.A.; Bhaskar, M.G.B.; Telang, M.D. Comparing the effect of earthquake on shear wall building and non-shear wall building—A review. *Int. Res. J. Eng. Technol.* **2017**, *4*, 3286–3289.
2. Ghosh, S.; Kharmale, S.B. Research on steel plate shear wall: Past, present and future. In *Structural Steel and Castings: Shapes and Standards, Properties and Applications*; Nova Science Publishers Inc.: Hauppauge, NY, USA, 2010.
3. Basler, K. Strength of plate girders in shear. *J. Struct. Div.* **1961**, *87*, 151–180. [CrossRef]
4. Porter, D.M.; Rockey, K.C.; Evans, H.R. The collapse behavior of plate girders loaded in shear. *Struct. Eng.* **1975**, *53*, 313–325.
5. Thorburn, L.J.; Kulak, G.L.; Montgomery, C.J. *Analysis of Steel Plate Shear Walls Structural Engineering Report No. 107*; Department of Civil Engineering, The University of Alberta: Edmonton, AB, Canada, 1983.
6. Habashi, H.R.; Alinia, M.M. Characteristics of the wall–frame interaction in steel plate shear walls. *J. Constr. Steel Res.* **2010**, *66*, 150–158. [CrossRef]
7. Driver, R.G.; Kulak, G.L.; Kennedy, D.L.; Elwi, A.E. Cyclic test of four-story steel plate shear wall. *J. Struct. Eng.* **1998**, *124*, 112–120. [CrossRef]
8. Astaneh-Asl, A. *Seismic Behavior and Design of Steel Shear Walls*; Structural Steel Educational Council: Moraga, CA, USA, 2001.
9. Stojadinovic, B.; Tipping, S. Structural testing of corrugated sheet steel shear walls. In Proceedings of the Nineteenth International Specialty Conference on Cold-Formed Steel Structures, St. Louis, MO, USA, 14–15 October 2008.

10. Sabouri-Ghomi, S.; Roberts, T.M. Nonlinear dynamic analysis of thin steel plate shear walls. *Comput. Struct.* **1991**, *39*, 121–127. [CrossRef]
11. Sabouri-Ghomi, S.; Roberts, T.M. Nonlinear dynamic analysis of steel plate shear walls including shear and bending deformations. *Eng. Struct.* **1992**, *14*, 309–317. [CrossRef]
12. Alinia, M.M.; Shirazi, R.S. On the design of stiffeners in steel plate shear walls. *J. Constr. Steel Res.* **2009**, *65*, 2069–2077. [CrossRef]
13. Alinia, M.M.; Habashi, H.R.; Khorram, A. Nonlinearity in the postbuckling behaviour of thin steel shear panels. *Thin-Walled Struct.* **2009**, *47*, 412–420. [CrossRef]
14. Tromposch, E.W.; Kulak, G.L. *Cyclic and Static Behaviour of Thin Panel Steel Plate Shear Walls*; Department of Civil Engineering, The University of Alberta: Edmonton, AB, Canada, 1987.
15. Caccese, V.; Elgaaly, M.; Chen, R. Experimental study of thin steel-plate shear walls under cyclic load. *J. Struct. Eng.* **1993**, *119*, 573–587. [CrossRef]
16. Hu, Y.; Zhao, J.; Jiang, L. Seismic risk assessment of steel frames equipped with steel panel wall. *Struct. Des. Tall Spec. Build.* **2017**, *26*, e1368. [CrossRef]
17. Li, G.; Wei, X.; Xiao, L.; Zhou, L. Numerical study on structural performance of corrugated steel plate shear wall with different yield points steel. *Struct. Des. Tall Spec. Build.* **2023**, *32*, e1996. [CrossRef]
18. Zhao, Q.; Sun, J.; Li, Y.; Li, Z. Cyclic analyses of corrugated steel plate shear walls. *Struct. Des. Tall Spec. Build.* **2017**, *26*, e1351. [CrossRef]
19. Emami, F.; Mofid, M. On the hysteretic behavior of trapezoidally corrugated steel shear walls. *Struct. Des. Tall Spec. Build.* **2014**, *23*, 94–104. [CrossRef]
20. Hosseinzadeh, L.; Mofid, M.; Aziminejad, A.; Emami, F. Elastic interactive buckling strength of corrugated steel shear wall under pure shear force. *Struct. Des. Tall Spec. Build.* **2017**, *26*, e1357. [CrossRef]
21. Wu, R.M.; Yu, C.Q.; Wang, L.Q.; Tong, J.Z. Shear elastic buckling of corrugated steel plate shear walls with stiffeners considering torsional rigidity. *Thin-Walled Struct.* **2025**, *206*, 112646. [CrossRef]
22. Tong, J.; Wu, R.; Wang, L. Experimental and numerical investigations on seismic behavior of stiffened corrugated steel plate shear walls. *Earthq. Eng. Struct. Dyn.* **2023**, *52*, 3551–3574. [CrossRef]
23. Yu, C.Q.; Tong, J.Z.; Zhang, J.M.; Tong, G.S.; Chen, M.; Xu, S.L.; Gao, W. Axial compressive behavior of multi-celled corrugated-plate CFST walls: Tests and numerical simulations. *Eng. Struct.* **2025**, *322*, 119033. [CrossRef]
24. Dou, C.; Ru, Y.; Jiang, Z.Q.; Wang, Y. Lateral resistant behavior of grid-reinforced steel corrugated shear walls. *J. Struct. Eng.* **2024**, *150*, 04024047. [CrossRef]
25. Bagherinejad, M.H.; Haghollahi, A. New form of perforated steel plate shear wall in simple frames using topology optimization. *J. Struct. Eng. Mech.* **2020**, *74*, 325–339.
26. Bagherinejad, M.H.; Haghollahi, A. Study on topology optimization of perforated steel plate shear walls in moment frame based on strain energy. *Int. J. Steel Struct.* **2020**, *20*, 1420–1438. [CrossRef]
27. Ghasemi Jouneghani, H.; Nouri, Y.; Mortazavi, M.; Haghollahi, A.; Memarzadeh, P. Seismic Performance Factors of Elliptic-Braced Frames with Rotational Friction Dampers through IDA. *J. Pract. Period. Struct. Des. Constr.* **2024**, *29*, 04024070. [CrossRef]
28. Jouneghani, H.G.; Nouri, Y.; Memarzadeh, P.; Haghollahi, A.; Hemati, E. Seismic performance and failure mechanisms evaluation of multi-story elliptic and mega-elliptic bracing frames: Experimental and numerical investigation. *J. Struct.* **2024**, *70*, 107658. [CrossRef]
29. Silva, M.J.; Gibson, L.J. The effects of non-periodic microstructure and defects on the compressive strength of two-dimensional cellular solids. *Int. J. Mech. Sci.* **1997**, *39*, 549–563. [CrossRef]
30. Hou, B.; Xiao, R.; Sun, T.F.; Wang, Y.; Liu, J.G.; Zhao, H.; Li, Y.L. A new testing method for the dynamic response of soft cellular materials under combined shear–compression. *Int. J. Mech. Sci.* **2019**, *159*, 306–314. [CrossRef]
31. Li, K.; Gao, X.L.; Subhash, G. Effects of cell shape and cell wall thickness variations on the elastic properties of two-dimensional cellular solids. *Int. J. Solids Struct.* **2005**, *42*, 1777–1795. [CrossRef]
32. Zhou, Q. Applications of cellular materials and structures in vehicle crashworthiness and occupant protection. In *Engineering Plasticity and Impact Dynamics*; World Scientific: Singapore, 2001; pp. 97–115.
33. Chen, L.; Tsopelas, P. Cellular-solid shear walls under seismic excitations. In Proceedings of the 9th US National Conference on Earthquake Engineering, Toronto, ON, Canada, 25–29 July 2010; pp. 25–29.
34. Vian, D.; Bruneau, M. Testing of special LYS steel plate shear walls. In Proceedings of the 13th Conference on Earthquake Engineering, Vancouver, BC, Canada, 1–6 August 2004.
35. Berman, J.; Bruneau, M. Plastic analysis and design of steel plate shear walls. *J. Struct. Eng.* **2003**, *129*, 1448–1456. [CrossRef]
36. Emami, F.; Mofid, M.; Vafai, A. Experimental study on cyclic behavior of trapezoidally corrugated steel shear walls. *Eng. Struct.* **2013**, *48*, 750–762. [CrossRef]
37. American Society of Civil Engineers. *Minimum Design Loads for Buildings and Other Structures*; American Society of Civil Engineers: Reston, VA, USA, 1996.

38. Applied Technology Council and National Earthquake Hazards Reduction Program (US). *Seismic Performance Assessment of Buildings*; Federal Emergency Management Agency: Washington, DC, USA, 2018.
39. AISC Committee. *Specification for Structural Steel Buildings*; ANSI/AISC 360-16; American Institute of Steel Construction: Chicago, IL, USA, 2016.
40. Sabelli, R.; Bruneau, M. *Design Guide 20: Steel Plate Shear Walls*; American Institute of Steel Construction: Chicago, IL, USA, 2007.